Journal of Biomechanical Engineering. Received April 29, 2020;
Accepted manuscript posted October 8, 2020. doi:10.1115/1.4048710

Predictions of anterior cruciate ligament dynamics from subject-specific musculoskeletal models and dynamic biplane radiography.

Authors

James P Charles[1,2], Freddie H. Fu[2] and William J Anderst[2]

[1]Evolutionary Morphology and Biomechanics Lab, Musculoskeletal Biology, University of Liverpool, UK.

[2] Biodynamics Lab, Department of Orthopaedic Surgery, University of Pittsburgh, PA, USA.

Corresponding Author:

James P Charles

Evolutionary Morphology and Biomechanics Lab

University of Liverpool

6 West Derby Street

Liverpool, UK

j.charles@liverpool.ac.uk

07891976240

Keywords:

Ligament force, knee, simulations, static optimization, joint reaction analysis

Journal of Biomechanical Engineering. Received April 29, 2020;
Accepted manuscript posted October 8, 2020. doi:10.1115/1.4048710

Abstract

In vivo knee ligament forces are important to consider for informing rehabilitation or clinical interventions. However, they are difficult to directly measure during functional activities. Musculoskeletal models and simulations have become the primary methods by which to estimate in vivo ligament loading. Previous estimates of anterior cruciate ligament (ACL) forces range widely, suggesting that individualized anatomy may have an impact on these predictions. Using 10 subject-specific (SS) lower limb musculoskeletal models, which include individualized musculoskeletal geometry, muscle architecture and 6 degree-of-freedom knee joint kinematics from dynamic biplane radiography, this study provides subject-specific estimates of ACL force (anteromedial- aACL; and posterolateral- pACL bundles) during the full gait cycle of treadmill walking. These forces are compared to estimates from scaled-generic (SG) musculoskeletal models to assess the effect of musculoskeletal knee joint anatomy on predicted forces and the benefit of subject-specific modelling in this context. On average, the SS models demonstrated a double force peak during stance (0.39 – 0.43 xBW per bundle), while only a single force peak during stance was observed in the SG aACL. No significant differences were observed between continuous SG and SS ACL forces, however root mean squared differences between SS and SG predictions ranged from 0.08 xBW to 0.27 xBW, suggesting SG models do not reliably reflect forces predicted by SS models. Force predictions were also found to be highly sensitive to ligament resting length, with ±10% variations resulting in force differences of up to 84%. Overall, this study demonstrates the sensitivity of ACL force predictions to subject-specific anatomy, specifically musculoskeletal joint geometry and ligament resting lengths, as well as the feasibility for generating subject-specific musculoskeletal models for a group of subjects to predict in vivo tissue loading during functional activities.

Journal of Biomechanical Engineering. Received April 29, 2020;
Accepted manuscript posted October 8, 2020. doi:10.1115/1.4048710

Introduction

Insights into knee ligament dynamics during gait, such as strains and passive forces, are crucial for understanding injury mechanisms and informing rehabilitations and clinical interventions following these injuries [1]. However, passive forces from these ligaments are very difficult to directly measure *in vivo* during dynamic activities such as gait, and as such have often been estimated using biomechanical modeling or similar methods [2-12]. These studies have reported a wide range of passive forces from the anterior cruciate ligament (ACL) during various functional activities, with estimates ranging from 0.5 x body weight (xBW) [13] to 3.5 xBW [6] during walking. There is clearly little consensus over exactly how much force is developed by the ACL during gait, with this large range of values suggesting that results are largely dependent on the level of complexity within the models, or the anatomy of the single individual upon which these models are often based. There is therefore justification for addressing the limitations of previous studies by using a cohort of subject-specific musculoskeletal models to predict ACL forces during gait in multiple subjects.

The benefits of patient-specific models relative to the more-often used scaled-generic models are becoming more accepted, with several studies reporting high sensitivity of models to individualized anatomical factors such as bone geometry, muscle attachment points and joint centers of rotation [14-23]. These models can be further improved by including precise multiple-degree-of-freedom (DoF) joint kinematics obtained from dynamic biplane radiography, which can replicate bone positions and orientations with sub-millimeter accuracy [24]. This can demonstrably improve the accuracy of musculoskeletal models compared to exclusively using traditional skin-mounted surface marker motion capture methods [25].

Regardless of how detailed these individualized models are, the accuracy of ligament force predictions is inherently dependent on the accuracy of their input parameters, particularly resting length (or the length beyond which these tissues begin generating passive forces). This however is a difficult measurement to obtain *in vivo* during dynamic movements such as gait, and as such is usually estimated in studies into knee ligament dynamics, for example, by using a

Journal of Biomechanical Engineering. Received April 29, 2020;
Accepted manuscript posted October 8, 2020. doi:10.1115/1.4048710

standardized correction percentage of 85% of the ligament's maximum length throughout the full knee flexion/extension range of motion, as described by Guess et al. [26].

This study aims to create a set of subject-specific lower limb musculoskeletal models using a validated framework [23, 27, 28] to estimate the passive forces exerted by the ACL during a full cycle of level treadmill walking in uninjured knees. The models will include individualized bone geometries, muscle attachments, joint centers of rotation, muscle force generating properties and 6 DoF knee joint kinematics from a biplane radiography system. The outputs from these models will be compared to those from corresponding scaled-generic models, which will give important insights into the sensitivity of ligament force predictions to patient-specific properties, the inter-subject variability in predicted passive forces in the aACL and pACL forces during gait, and the necessity of creating subject-specific models for answering detailed clinical questions in future studies. Furthermore, a sensitivity analysis where ligament resting lengths will be altered to test the effect on predicted passive forces will give insight into the importance of this parameter in obtaining individualized predictions of knee joint dynamics during gait. These analyses will be used to address two hypotheses: 1) due to the inclusion of individualized bone and muscle data, the subject-specific musculoskeletal models will produce significantly different and more plausible and precise predictions of knee ligament dynamics relative to their scaled-generic equivalents; and 2) predictions of passive knee ligament forces will be highly sensitive to resting length input values.

Methods

Subject-specific model construction

To create the subject-specific (SS) lower limb musculoskeletal models (Figure 1), musculoskeletal geometry of the right lower limbs of ten individuals (5 males, 5 females; Age- 27 ± 4 years; Body mass- 76 ± 12 kg) was obtained from magnetic resonance imaging (MRI). Each subject signed informed consent prior to taking part in this IRB approved study. Imaging primarily consisted of three sequences: T1-weighted anatomical turbo spin echo (voxel size 0.47 × 0.47 × 6.5 mm^3, repetition time [TR] - 650 ms, echo time [TE] - 23 ms, number of slices - 35 per segment, number of signal averages (NSA) - 1, acceleration factor - 2) to image from the iliac crest to the ankle joint;

Journal of Biomechanical Engineering. Received April 29, 2020;
Accepted manuscript posted October 8, 2020. doi:10.1115/1.4048710

T2 (sagittal, voxel size- $0.29 \times 0.29 \times 0.59$ mm^3, TR – 29ms, TE – 16ms, NSA- 1) to image the knee joint ±7.5cm above and below the joint line; and diffusion-weighted single-shot dual-refocusing spin-echo planar (voxel size $2.96 \times 2.96 \times 6.5$ mm^3, TR/TE 7900/65 ms, 12 direction diffusion gradients, *b* value - 0 & 400 s/mm^2, strong fat suppression - spectral attenuated inversion recovery [SPAIR], number of slices - 35 per segment, NSA - 2, acceleration factor - 2, bandwidth - 2440 Hz/pixel) to determine *in vivo* muscle fiber lengths and pennation angles using a validated framework of fiber tractography. See Charles et al. [28] for details of this method, and Charles et al. [27] for an extensive data set of *in vivo* lower limb muscle architecture from the same individuals in this study. All subjects were imaged in a supine position in the same 3 T scanner (Biograph mMR, Siemens, Munich, Germany), with a total scanning time of ~37 minutes.

The T1 MR images were digitally segmented in Mimics (Materalise, Leuven, Belgium) to create 3D volumetric meshes of 20 lower limb muscles, as well as the pelvic bones, femur, tibia, fibula and foot bones. The T2 MR images were similarly segmented to create detailed 3D meshes of the distal femur, proximal tibia and fibula, patella and the ACL. The meshes of the femur, tibia and fibula bones segmented from the T1 and T2 MR images were each merged, to create full bone models with detailed articular surfaces at the knee.

Each subject-specific lower limb model was assembled in NMSBuilder [29]. Muscle force generating properties for 21 musculotendon unit (MTU) models were derived from a previously published data set of *in vivo* muscle anatomy from the same subjects used in this study [27], which was generated using a combination of anatomical MRI and diffusion tensor imaging (DTI). Including subject-specific muscle force generating properties derived from DTI fiber tractography has been shown to significantly improve the accuracy of model outputs relative to using more generic data [23], and so was included in the models here to optimize their subject-specificity and accuracy. The points of origins and insertions and via points for these MTUs were placed based on the 3D muscle meshes segmented from the T1 MR images (Table 1). The Adductor magnus muscle was represented by two MTUs (lateral and medial) due to its broad origin on the ischium and two insertions on the medial femur separated by the adductor foramen. To account for this, maximum isometric force of the whole muscle [27] was split evenly between these MTUs, while optimal fiber length and pennation angle remained the same, which is common practice in

Journal of Biomechanical Engineering. Received April 29, 2020;
Accepted manuscript posted October 8, 2020. doi:10.1115/1.4048710

musculoskeletal modeling [21, 30-32]. See Tables S1-S10 for the force generating properties included in each individual musculoskeletal model. This method of attachment point placement is similar to that described previously and has an overall median error of 6.1mm along all 3 axes [15].

Ligament model properties

Attachment points of the ACL were determined from 3D meshes from the T2 MR images, as described by Nagai et al. [33]. Similar to Nagai et al. [33], and to ensure consistency with current musculoskeletal models which include knee ligaments [34], the ACL was modeled by two ligament models representing the anteromedial bundle (aACL) and posterolateral bundle (pACL) in each subject. The dynamic properties of the ligaments were modeled as described by Stanev et al. [35], where input parameters include the ligament's resting length (L_r), stiffness and damping. Stiffness and damping values were taken from previous literature [34] and were consistent between all subjects (1500N and 390N respectively for the aACL, and 1600N and 403N for the pACL), while L_r values were estimated for both bundles in each subject using a standardized correction percentage [26, 36]. These resting lengths are shown in Tables 2 and 3.

Wrap surfaces were added to the model to prevent muscles passing through bones surfaces (Table 1), and were placed based on those in a generic full body OpenSim model [37] and subsequently manually optimized in size and location to minimize muscle-bone penetration during joint rotations. Coordinate systems and joint centers for the hip, knee and ankle joints were determined based on the lower extremity anatomical landmark sets recommended by the International Society of Biomechanics [38] (Figure 2). Each model was exported to Opensim 3.3 [39] for further analysis.

Data collection

Lower limb joint kinematics and kinetics were gathered from the same 10 individuals (Figure 3) with a 12-camera motion capture system (Vicon vantage, Oxford, UK; 100Hz) measuring full-body motion for one whole stride (heel strike to heel strike) of level treadmill walking (4 trials, 13 seconds at 1.5ms^{-1}). A total of 55 reflective markers were placed on each subject.

Journal of Biomechanical Engineering. Received April 29, 2020;
Accepted manuscript posted October 8, 2020. doi:10.1115/1.4048710

A customized dynamic biplane radiography (DBR) system imaged the knee joint through these same walking steps (100Hz), with two trials recording one half of the gait cycle (mid-swing to mid-stance), and two recording the other half (mid-stance to mid-swing). Ground reaction forces (GRFs) were recorded using a dual-belt instrumented treadmill (Bertec Corporation, Columbus, Ohio).

High resolution CT scans (voxel size- 0.6 × 0.6 × 0.6 mm) of both knee joints were then collected for each individual. The acquired CT images were then digitally segmented (Mimics 17.0, Materalise) to obtain models of the femur and tibia bones. A validated volumetric model-based tracking process determined the precise three-dimensional (3D) six degree of freedom knee joint kinematics (Figure 4) through the recorded walking steps using the biplane radiographs and digitally reconstructed radiographs [24]. The kinematics from the four walking trials for each subject were averaged and then combined to obtain full gait cycle, 6 degree of freedom knee joint kinematics. See Gale, et al. [40] for full details regarding the acquisition and analysis of these knee joint kinematics from the DBR system. Motion capture marker coordinates and GRF data (low-pass filtered at 20Hz) were processed and prepared for subsequent modeling steps using the freely available "C3D extraction toolbox" for MATLAB (https://simtk.org/home/c3d2opensim_btk).

Simulations

For each subject-specific lower limb model, the standard OpenSim simulation protocol of inverse kinematics (IK) and residual reduction algorithm (RRA) was applied. The IK step was modified to allow for the predefined knee joint kinematics from DBR to be combined with the hip and ankle joint kinematics from motion capture marker positions. Static optimization was used to estimate knee ligament forces during walking, with the objective function of minimizing the sum of muscle activations squared.

An initial validation of each SS model was performed by comparing predicted knee joint loads to previously published *in vivo* knee joint forces [41]. The model predictions of joint contact force were obtained using the Joint Reaction Analysis within OpenSim 3.3, while *in vivo* forces were

Journal of Biomechanical Engineering. Received April 29, 2020;
Accepted manuscript posted October 8, 2020. doi:10.1115/1.4048710

measured during treadmill walking in 6 individuals with instrumented knee joint replacements (24 total gait cycles; 1.1ms^{-1}, sports shoes. Data available at www.orthload.com).

Full body generic musculoskeletal models [37] were then scaled to match the anthropometry of each subject. The same simulation protocol was applied to these scaled generic (SG) models, which provided direct comparisons to the subject-specific models. In these models, the muscle and ligament attachment sites remained unchanged from their default settings. Resting lengths in the aACL and pACL were altered using the same correction percentage applied to the subject-specific models.

Data analysis

Ligament forces predicted from static optimization in SG and SS models were normalized to body weight (xBW) for comparison. A paired t-test was used to test for significant differences between aACL and pACL forces predicted by the SS (F_{SS}) and SG (F_{SG}) models at all time points of the gait cycle using the freely available statistical parametric mapping (SPM) toolbox [42]. Here, this calculation reported statistically significant differences (p<0.05) when the *t* statistic, also referred to as SPM{t} [42], exceeded a threshold value. These thresholds were > 4.18 or < -4.18 for the aACL, and > 4.37 or < -4.37 for the pACL.

To quantify the agreement of the ligament forces predicted in both ACL bundles by the SG models relative to the SS models, root mean squared (RMS) differences were calculated for each subject through the entire walking gait cycle ($\sqrt{\overline{(F_{SS} - F_{SG})^2}}$). Intra-subject variability in predicted ACL bundle forces was quantified by the average standard deviation of those forces throughout the gait cycle.

Sensitivity analysis

To test the effect of predictions of knee ligament forces to uncertainties in resting length values, these values in the aACl and pACL were altered ±10% of their initial value within the SS models (see Tables 2 and 3). Static optimization was then re-run for each SS model within OpenSim to predict the resulting ligament forces.

Journal of Biomechanical Engineering. Received April 29, 2020;
Accepted manuscript posted October 8, 2020. doi:10.1115/1.4048710

Results

Ligament forces

Subject-specific simulations predicted a double peak of knee ligament forces in both the aACL and pACL during a walking gait cycle (Fig. 5 A, B). The first peak occurred at early stance phase, and the second peak occurred during mid-late stance phase. There was also an increase in ligament force at the end of the swing phase, just prior to heel strike. These peaks appear to correspond to peaks of ligament strain measured previously within the same individuals (Nagai et al 2019) (see Figure 5). Average force in the aACL was 0.42 ± 0.05 xBW at the first peak, and 0.43 ± 0.05 xBW at the second peak in the SS models. In the pACL, average force was 0.38 ± 0.06 xBW at the first peak, and 0.41 ± 0.06 xBW at the second peak. Inter-subject variability in aACL and pACL forces predicted by the SS models averaged 0.14 xBW and 0.13 xBW respectively, over the entire gait cycle (Figure 5).

Scaled generic models predicted a similar double-peaked behavior during walking in the pACL (Fig. 5 B), and similar peak forces as in the SS models (0.38 ± 0.04 at the first peak, and 0.39 ± 0.07 at the second peak). This was not seen in the aACL (Fig. 5 A), which exhibited only one peak of force during midstance (at around 0.41 ± 0.05 xBW on average), with only a slight reduction in force through the swing phase (Figure 5 A). In the SG models, inter-subject variability averaged 0.15 xBW in both the aACL and the pACL over the gait cycle (Figure 5).

SPM showed no statistically significant differences between forces predicted by the SS and SG models in either the aACL or the pACL throughout the entire gait cycle (Figure 5 C, D). However, individual subject RMS difference values showed substantial variability between individuals, with differences between SS and SG simulations ranging from 0.08 xBW (21.1% of maximum force; Subject 1) to 0.26 xBW (30.6%; Subject 8) in the aACL, and from 0.05 xBW (17%; Subject 10) to 0.18 xBW (43.3%; Subject 3) in the pACL (Table 4).

Sensitivity analysis

Altering the resting lengths of both the aACL and pACL in the subject-specific models had substantial effects on predictions of force during walking (Figure 6). Increasing resting lengths by

Journal of Biomechanical Engineering. Received April 29, 2020;
Accepted manuscript posted October 8, 2020. doi:10.1115/1.4048710

10% resulted in decreases of peak forces up to 0.18 xBW (57% change) and 0.13 xBW (65%) at the first force peak during the stance phase in the aACL and pACL respectively. Similar reductions in peak forces were seen at the second peak (54% and 60% in the aACL and pACL respectively). Reducing ligament resting lengths by 10% resulted in large increases in peak forces in the aACL and pACL. In the early stance phase, peak forces increased by 69% and 73% in the aACL and pACL respectively (increased to 0.71 and 0.66 xBW). In the late stance phase, peak aACL force increased by 71% (to 0.72 xBW), while peak pACL increased by 84% (to 0.70 xBW).

Knee joint contact forces

Predicted knee joint contact forces followed similar patterns in the SS models to those measured *in vivo* [41], and peak forces were similar, with forces of ~3 xBW in the SS models and ~2.3 xBW in the *in vivo* data (Figure 7).

Discussion

The main goal of this study was to compare high-fidelity subject-specific musculoskeletal models to scaled generic models of the lower limb for predicting anterior cruciate ligament dynamics during gait. Secondary goals were to quantify the sensitivity of ligament forces predictions to variations in individualized musculoskeletal and ligament anatomy and to characterize the among-subject variability in predicted ACL forces during gait. Two hypotheses were formulated to attempt to achieve these goals, where it was hypothesized that 1) due to the inclusion of individualized bone and muscle data, the subject-specific musculoskeletal models will produce significantly different and more plausible and precise predictions of knee ligament dynamics relative to their scaled-generic equivalents; and 2) predictions of passive knee ligament forces will be highly sensitive to resting length input values.

Previous plausible estimates of peak ACL force during walking range from 0.5 - 1.7 xBW [2, 5, 7-12], which model the ACL as one whole structure. Our peak force estimates from the SS and SG models, which model the ACL as two bundles, fall within this range when forces from both bundles are summed to provide a total force from the entire ACL structure (0.80 – 0.84 xBW). It is important to note that these ACL force values are the average over our entire group of 10 subjects, which showed variability in peak force that ranged from 0.32 to 0.87 xBW (in the aACL).

Journal of Biomechanical Engineering. Received April 29, 2020;
Accepted manuscript posted October 8, 2020. doi:10.1115/1.4048710

This large range of values (and standard deviations) points to a potentially large inter-subject variability in ACL forces, and suggest that previous studies have not necessarily provided incorrect predictions of forces but have instead been limited by their relatively small sample sizes. The ability of a valid subject-specific modeling framework to capture inter-subject variations in musculoskeletal anatomy, and by extension musculoskeletal and ligament function, is an inherent advantage of this method over generic or scaled generic models, however, in the absence of a "gold standard" reference for *in vivo* knee ligament forces, these estimates are difficult to validate.

The patterns of ligament forces in both ACL bundles predicted here in the SS models follow the patterns of relative elongation reported by Nagai et al. [33], whose analyses used the same subjects. Nagai et al. [33] showed two relative elongation peaks during the stance phase and a peak towards terminal swing phase in both bundles, with the relative elongation of the aACL higher than that of the pACL, which is also similar to the forces seen here. These patterns are however different to those seen in previous models and predictions of ACL dynamics [2-4, 12], some of which predicted two peaks of relative strain or elongation, at mid-late stance phase and terminal swing phase. Potential reasons for these differences may be due to more accurate kinematics relative to Taylor et al. [4] and higher walking speeds relative to Wu, et al. [3] (see Nagai, et al. [33] for further discussion of these differences).

However, while the SS models exhibited similarities to previous data, the SG models did not, particularly in the aACL, where a double force peak during stance was not observed and forces remained high throughout the swing phase. Despite the peak force being within a physiological range, and the differences from the SS models not being statistically significant throughout the gait cycle, the peak force during midstance and relatively high loading throughout the swing phase are unlikely to be representative of true aACL dynamic behavior during walking. Therefore, these data partially supported Hypothesis 1, although it is possible that small adjustments to the ligament attachment points within the scaled-generic models, particularly those of the aACL, could improve the force predictions of the scaled-generic models and result in closer matches to the subject-specific predictions.

Journal of Biomechanical Engineering. Received April 29, 2020;
Accepted manuscript posted October 8, 2020. doi:10.1115/1.4048710

However, this good agreement in ligament forces between the model types did not appear to be consistent across all the subjects in this study. The large variation in RMS difference values between the subjects (ranging from 0.08 xBW to 0.27 xBW in the aACL) showed that the SG models lack precision in predicting knee ligament dynamics in subjects with a range of anthropometries. There are many potential reasons for this variability in the accuracy of the SG models, such as inconsistencies in scaling and discrepancies in ligament attachment points. The attachment point location (onto the femur and tibia) and orientation of the ACL are known to vary considerably between individuals due to variations in the anatomy of the knee joint complex [43], and these are important factors which cannot be precisely incorporated into scaled-generic models. Given that ligament resting lengths in the SG models were determined with the same correction percentage to the SS models, but attachment sites coordinates remained unchanged from their generic values, these discrepancies in force highlight the importance of accurately identifying and incorporating individualized ligament attachment sites into musculoskeletal models in order to accurately estimate ligament forces during gait. This sensitivity of knee ligament forces to origin and insertion location was also suggested by Beynnon, et al. [44] and lends further support to the use of subject-specific musculoskeletal modeling within clinical or sports biomechanics, where high resolution MR images can be used to determine individualized muscle and ligament geometry. Within these fields, a valid framework to generate high fidelity predictive models of the knee joint complex in a range of subjects provides a platform upon which to test various functional hypotheses of *in vivo* tissue loading, and could also be used to generate personalized predictions of post-surgical outcomes or inform tailored injury rehabilitation protocols.

Ligament resting lengths

The comparison between subject-specific and scaled generic models suggests that estimates of ligament dynamics are highly sensitive to attachment sites and bony geometry. However, the resting length of these ligaments (the length beyond which they begin to develop a passive force) is another important input factor into these ligament models, but one which is usually estimated rather than directly measured in studies modelling the dynamic behavior of knee ligaments. The results of the sensitivity analysis, where initial resting length values were changed ±10%,

Journal of Biomechanical Engineering. Received April 29, 2020;
Accepted manuscript posted October 8, 2020. doi:10.1115/1.4048710

supported Hypothesis 2 and quantified the high sensitivity of force predictions to uncertainties in certain input values, with a 10% decrease in resting length resulting in increases in peak passive forces of up to 84% from the pACL during the late stance phase. Using estimates of resting lengths is an inherent limitation of studies modelling knee ligament dynamics due to difficulty in obtaining such values *in vivo*, with the “optimal” approach currently being calculating this value using a correction percentage based on maximum ligament length [26, 36]. While various medical imaging techniques such as ultrasound, shearwave or magnetic resonance elastography have shown promise as potential methods for obtaining *in vivo* estimates of ligament resting lengths, as well as other *in vivo* muscle/tendon parameters [45-49], they may prove unsuitable for obtaining similar parameters from the ACL due to occlusion from the femoral condyles or tibial plateau. It is therefore likely that estimating resting lengths will remain the most feasible method of enabling individualized predictions of knee ligament dynamics using musculoskeletal modeling, but one which can be optimized with knowledge of individualized ligament geometry obtained through subject-specific modeling.

It should be noted that while attempts were made to individualize the resting length values of the ACL in each model, the stiffness and damping values remained unchanged from their generic values [34]. This was due to a lack of knowledge about how these parameters vary between individuals and further difficulty in measuring these *in vivo*, but regardless reduced the subject-specificity of each model. These assumptions further contributed to what could be seen as a relatively simple model of ligament dynamics used here [35], particularly when compared to more complex models such as that described by Nasseri, et al. [50]. However, the model developed by Stanev, et al. [35] has the advantage of being easily incorporated into the open-source, user friendly OpenSim modeling environment, meaning it can be readily used in a range of studies to accurately predict ligament dynamics in multiple individuals, which this study succeeded in demonstrating.

Limitations

Journal of Biomechanical Engineering. Received April 29, 2020;
Accepted manuscript posted October 8, 2020. doi:10.1115/1.4048710

While this study represents an initial and important insight into the necessity of detailed subject-specific modeling and kinematics in estimating knee ligament dynamics, a few limitations and assumptions inherent to musculoskeletal modeling hinder the clinical relevance of these findings.

As mentioned, *in vivo* measurements of knee ligament forces are impossible to obtain during dynamic activities such as walking. Therefore, while a good agreement in predicted ACL forces was seen in the SS models to previous musculoskeletal modeling studies, comparisons such as these do little to assess the true validity of the models or their outputs. But good matches between predicted knee joint loads in the SS models relative to *in vivo* data raised confidence in this modeling framework and in the model's functional predictions, and suggested that they were accurately replicating the dynamics of the knee joint complex. Of course, an exact match between knee joint forces predicted from models of young, healthy individuals and those measured from older individuals with knee joint replacements should not be expected, due to differences in age, gait kinematics and walking speed (1.5ms^{-1} vs. 1.1 ms^{-1}). Therefore, the lack of *in vivo* data against which to truly compare predictions of ligament forces from musculoskeletal models make validation attempts difficult and may limit their immediate clinical applicability. However, it is possible that incorporating an improved ligament model into these musculoskeletal models, such as that described by Nasseri, et al. [50] which was validated against cadaveric data obtained through a drop-landing task, could raise confidence in the force predictions generating using this subject-specific modeling framework.

Despite the high accuracy of the knee joints in each subject-specific model created here, with high resolution musculoskeletal geometry, 6 degrees of joint freedom and individualized joint centers of rotation based on anatomical landmarks, these centers of rotation were fixed throughout each walking gait cycle. There are questions regarding how this assumption affects the accuracy of predicted model outcomes, as van den Bogert, et al. [51] showed that knee joint center of rotation moves and changes orientation substantially during gait, which could have a large effect on muscle and ligament moment arms. While implementing a moving center of knee joint rotation within the OpenSim subject-specific modeling framework presented here was out of the scope of this study, doing so could provide more realistic personalized predictions of muscle and ligament forces in future studies.

Journal of Biomechanical Engineering. Received April 29, 2020;
Accepted manuscript posted October 8, 2020. doi:10.1115/1.4048710

Our study focused on level treadmill walking, however investigating downhill running, cutting or pivot maneuvers, which place more load on the ACL would be more relevant to predictions of post-surgical rehabilitation. Furthermore, given that the force from both ACL bundles seen here was homogenous, something also noted by Wu, et al. [3] during walking, analyzing more demanding movements may give further insights into the dynamic differences between the aACL and pACL bundles. These two bundles have also been seen to wrap over each other during knee flexion-extension [52], however ligament wrapping was not included in this study. Ultrasound imaging of the ACL could also provide insights into how the two bundles interact during knee rotations and translations and may allow more accurate representations of this behavior in musculoskeletal models using wrapping surfaces.

Future directions

Here we establish an efficient framework for developing highly detailed subject-specific lower limb musculoskeletal models and simulations of knee ligament dynamics which incorporate individualized musculoskeletal geometry, muscle architecture and high precision knee joint kinematics from dynamic biplane radiographs.

Predictions of ACL forces from the subject-specific models through walking are slightly lower than values reported in previous literature, although without “gold-standard” reference values of *in vivo* ligament forces, it is assumed that these values are not physiologically unfeasible during a low-demand movement such as walking. The more physiologically plausible and precise predictions of ACL dynamics predicted by the subject-specific models relative to the scaled-generic models, as well as the high sensitivity of these predictions to ligament input parameters, support the need for a high degree of personalization in models such as these for clinical uses. However, further study and refinements to this framework are needed before these models can be used clinically. More accurate measurements of ACL resting lengths, or the use of more complex ligament models, will optimize predictions of its dynamic behavior during gait, and attempts to automate the process of creating the subject-specific models are crucial for applying this framework to clinical cases. Nevertheless, this study provides solid support to the notion that highly accurate subject-specific musculoskeletal models can be developed for groups of

Journal of Biomechanical Engineering. Received April 29, 2020;
Accepted manuscript posted October 8, 2020. doi:10.1115/1.4048710

individuals (healthy or pathological) and used within freely available musculoskeletal modelling software for hypothesis testing related to post-surgical ligament dynamics. This is particularly important for future work, as while it is possible to predict ligament forces without the creation of detailed inverse dynamics based musculoskeletal models, generating predictive simulations of functional post-surgical and rehabilitation outcomes cannot be done using purely kinematics-based methods. Furthermore, a large set of individualized models such as that presented here would also be an ideal platform upon which to investigate the relationships between musculoskeletal anatomy, physiology and ligament forces, which could help to increase understanding surrounding ACL injury risk factors in various patient populations. Furthermore, if these methods were to be applied to other joints, this could lead to an extensive set of highly detailed subject-specific models of the human musculoskeletal system with potentially greater clinical applicability than scaled-generic models.

Conflicts of Interest

No benefits in any form have been or will be received from a commercial party related directly or indirectly to the subject of this manuscript.

Acknowledgements

This research was funded in part by Grant #2R44HD066831-02A1 from the NIH and in part internally by the Department of Orthopaedic Surgery at the University of Pittsburgh. The authors would like to thank Chan Hong Moon of the University of Pittsburgh Magnetic Resonance Research Center for invaluable assistance in developing the MRI sequences necessary to sufficiently image the lower limb musculoskeletal system for creation of the musculoskeletal models, as well as Milad Zarei and Tom Gale of the Biodynamics Lab for assisting in kinematic data collection and processing. We also thank the three peer reviewers for their valuable comments which helped to improve the manuscript.

Author Contributions

Journal of Biomechanical Engineering. Received April 29, 2020;
Accepted manuscript posted October 8, 2020. doi:10.1115/1.4048710

Conceived study: JPC, FHF, WJA; Kinematic data collection, MRI acquisition, and model creation and analysis: JPC; Drafted and revised manuscript: JPC, FHF, WJA.

References

[1] Fleming, B. C., and Beynnon, B. D., 2004, "In vivo measurement of ligament/tendon strains and forces: a review," Ann Biomed Eng, 32(3), pp. 318-328.
[2] Shelburne, K. B., Pandy, M. G., Anderson, F. C., and Torry, M. R., 2004, "Pattern of anterior cruciate ligament force in normal walking," J Biomech, 37(6), pp. 797-805.
[3] Wu, J. L., Hosseini, A., Kozanek, M., Gadikota, H. R., Gill, T. J. t., and Li, G., 2010, "Kinematics of the anterior cruciate ligament during gait," Am J Sports Med, 38(7), pp. 1475-1482.
[4] Taylor, K. A., Cutcliffe, H. C., Queen, R. M., Utturkar, G. M., Spritzer, C. E., Garrett, W. E., and DeFrate, L. E., 2013, "In vivo measurement of ACL length and relative strain during walking," J Biomech, 46(3), pp. 478-483.
[5] Toutoungi, D. E., Lu, T. W., Leardini, A., Catani, F., and O'Connor, J. J., 2000, "Cruciate ligament forces in the human knee during rehabilitation exercises," Clin Biomech (Bristol, Avon), 15(3), pp. 176-187.
[6] Collins, J. J., and O'Connor, J. J., 1991, "Muscle-ligament interactions at the knee during walking," Proc Inst Mech Eng H, 205(1), pp. 11-18.
[7] Collins, J. J., 1995, "The redundant nature of locomotor optimization laws," J Biomech, 28(3), pp. 251-267.
[8] Serpas, F., Yanagawa, T., and Pandy, M., 2002, "Forward-dynamics simulation of anterior cruciate ligament forces developed during isokinetic dynamometry," Comput Methods Biomech Biomed Engin, 5(1), pp. 33-43.
[9] Shelburne, K. B., and Pandy, M. G., 1997, "A musculoskeletal model of the knee for evaluating ligament forces during isometric contractions," J Biomech, 30(2), pp. 163-176.
[10] Shelburne, K. B., and Pandy, M. G., 1998, "Determinants of cruciate-ligament loading during rehabilitation exercise," Clin Biomech (Bristol, Avon), 13(6), pp. 403-413.
[11] Shelburne, K. B., and Pandy, M. G., 2002, "A dynamic model of the knee and lower limb for simulating rising movements," Comput Methods Biomech Biomed Engin, 5(2), pp. 149-159.
[12] Moissenet, F., Cheze, L., and Dumas, R., 2014, "A 3D lower limb musculoskeletal model for simultaneous estimation of musculo-tendon, joint contact, ligament and bone forces during gait," J Biomech, 47(1), pp. 50-58.
[13] Harrington, I. J., 1976, "A bioengineering analysis of force actions at the knee in normal and pathological gait," Biomed Eng, 11(5), pp. 167-172.
[14] Scheys, L., Spaepen, A., Suetens, P., and Jonkers, I., 2008, "Calculated moment-arm and muscle-tendon lengths during gait differ substantially using MR based versus rescaled generic lower-limb musculoskeletal models," Gait Posture, 28(4), pp. 640-648.
[15] Scheys, L., Loeckx, D., Spaepen, A., Suetens, P., and Jonkers, I., 2009, "Atlas-based non-rigid image registration to automatically define line-of-action muscle models: a validation study," J Biomech, 42(5), pp. 565-572.
[16] Scheys, L., Desloovere, K., Suetens, P., and Jonkers, I., 2011, "Level of subject-specific detail in musculoskeletal models affects hip moment arm length calculation during gait in pediatric subjects with increased femoral anteversion," J Biomech, 44(7), pp. 1346-1353.
[17] Valente, G., Pitto, L., Testi, D., Seth, A., Delp, S. L., Stagni, R., Viceconti, M., and Taddei, F., 2014, "Are subject-specific musculoskeletal models robust to the uncertainties in parameter identification?," PLoS One, 9(11), p. e112625.

Journal of Biomechanical Engineering. Received April 29, 2020;
Accepted manuscript posted October 8, 2020. doi:10.1115/1.4048710

[18] Prinold, J. A., Mazzà, C., Di Marco, R., Hannah, I., Malattia, C., Magni-Manzoni, S., Petrarca, M., Ronchetti, A. B., Tanturri de Horatio, L., van Dijkhuizen, E. H., Wesarg, S., Viceconti, M., and Consortium, M.-P., 2016, "A Patient-Specific Foot Model for the Estimate of Ankle Joint Forces in Patients with Juvenile Idiopathic Arthritis," Ann Biomed Eng, 44(1), pp. 247-257.

[19] Ackland, D. C., Lin, Y. C., and Pandy, M. G., 2012, "Sensitivity of model predictions of muscle function to changes in moment arms and muscle-tendon properties: a Monte-Carlo analysis," J Biomech, 45(8), pp. 1463-1471.

[20] Navacchia, A., Myers, C. A., Rullkoetter, P. J., and Shelburne, K. B., 2016, "Prediction of In Vivo Knee Joint Loads Using a Global Probabilistic Analysis," J Biomech Eng, 138(3), p. 4032379.

[21] Charles, J. P., Cappellari, O., Spence, A. J., Wells, D. J., and Hutchinson, J. R., 2016, "Muscle moment arms and sensitivity analysis of a mouse hindlimb musculoskeletal model," J Anat, 229(4), pp. 514-535.

[22] Imani Nejad, Z., Khalili, K., Hosseini Nasab, S. H., Schutz, P., Damm, P., Trepczynski, A., Taylor, W. R., and Smith, C. R., 2020, "The Capacity of Generic Musculoskeletal Simulations to Predict Knee Joint Loading Using the CAMS-Knee Datasets," Ann Biomed Eng.

[23] Charles, J. P., Grant, B., D'Août, K., and Bates, K. T., 2020, "Subject-specific muscle properties from diffusion tensor imaging significantly improve the accuracy of musculoskeletal models," Journal of Anatomy, n/a(n/a).

[24] Anderst, W., Zauel, R., Bishop, J., Demps, E., and Tashman, S., 2009, "Validation of three-dimensional model-based tibio-femoral tracking during running," Med Eng Phys, 31(1), pp. 10-16.

[25] Zheng, L., Li, K., Shetye, S., and Zhang, X., 2014, "Integrating dynamic stereo-radiography and surface-based motion data for subject-specific musculoskeletal dynamic modeling," J Biomech, 47(12), pp. 3217-3221.

[26] Guess, T. M., Liu, H., Bhashyam, S., and Thiagarajan, G., 2011, "A multibody knee model with discrete cartilage prediction of tibio-femoral contact mechanics," Comput Methods Biomech Biomed Engin, 16(3), pp. 256-270.

[27] Charles, J. P., Suntaxi, F., and Anderst, W. J., 2019, "In vivo human lower limb muscle architecture dataset obtained using diffusion tensor imaging," PLoS One, 14(10), p. e0223531.

[28] Charles, J. P., Moon, C. H., and Anderst, W., 2019, "Determining subject-specific lower-limb muscle architecture data for musculoskeletal models using diffusion tensor MRI," J Biomech Eng, 141(6), pp. 060905-060905-060909.

[29] Valente, G., Crimi, G., Vanella, N., Schileo, E., and Taddei, F., 2017, "nmsBuilder: Freeware to create subject-specific musculoskeletal models for OpenSim," Comput Methods Programs Biomed, 152, pp. 85-92.

[30] Delp, S. L., Loan, J. P., Hoy, M. G., Zajac, F. E., Topp, E. L., and Rosen, J. M., 1990, "An interactive graphics-based model of the lower extremity to study orthopaedic surgical procedures," IEEE Trans Biomed Eng, 37(8), pp. 757-767.

[31] Van der Helm, F. C., Veeger, H. E., Pronk, G. M., Van der Woude, L. H., and Rozendal, R. H., 1992, "Geometry parameters for musculoskeletal modelling of the shoulder system," J Biomech, 25(2), pp. 129-144.

[32] Arnold, E. M., Ward, S. R., Lieber, R. L., and Delp, S. L., 2010, "A model of the lower limb for analysis of human movement," Ann Biomed Eng, 38(2), pp. 269-279.

[33] Nagai, K., Gale, T., Chiba, D., Su, F., Fu, F., and Anderst, W., 2019, "The Complex Relationship Between In Vivo ACL Elongation and Knee Kinematics During Walking and Running," J Orthop Res, 37(9), pp. 1920-1928.

[34] Xu, H., Bloswick, D., and Merryweather, A., 2015, "An improved OpenSim gait model with multiple degrees of freedom knee joint and knee ligaments," Comput Methods Biomech Biomed Engin, 18(11), pp. 1217-1224.

Journal of Biomechanical Engineering. Received April 29, 2020;
Accepted manuscript posted October 8, 2020. doi:10.1115/1.4048710

[35] Stanev, D., Moustakas, K., Gliatis, J., and Koutsojannis, C., 2016, "ACL Reconstruction Decision Support. Personalized Simulation of the Lachman Test and Custom Activities," Methods Inf Med, 55(1), pp. 98-105.

[36] Bloemker, K. H., Guess, T. M., Maletsky, L., and Dodd, K., 2012, "Computational knee ligament modeling using experimentally determined zero-load lengths," Open Biomed Eng J, 6, pp. 33-41.

[37] Rajagopal, A., Dembia, C. L., DeMers, M. S., Delp, D. D., Hicks, J. L., and Delp, S. L., 2016, "Full-Body Musculoskeletal Model for Muscle-Driven Simulation of Human Gait," IEEE Trans Biomed Eng, 63(10), pp. 2068-2079.

[38] Wu, G., Siegler, S., Allard, P., Kirtley, C., Leardini, A., Rosenbaum, D., Whittle, M., D'Lima, D. D., Cristofolini, L., Witte, H., Schmid, O., Stokes, I., Standardization, and Terminology Committee of the International Society of, B., 2002, "ISB recommendation on definitions of joint coordinate system of various joints for the reporting of human joint motion--part I: ankle, hip, and spine. International Society of Biomechanics," J Biomech, 35(4), pp. 543-548.

[39] Delp, S. L., Anderson, F. C., Arnold, A. S., Loan, P., Habib, A., John, C. T., Guendelman, E., and Thelen, D. G., 2007, "OpenSim: open-source software to create and analyze dynamic simulations of movement," IEEE Trans Biomed Eng, 54(11), pp. 1940-1950.

[40] Gale, T., and Anderst, W., 2019, "Asymmetry in healthy adult knee kinematics revealed through biplane radiography of the full gait cycle," J Orthop Res, 37(3), pp. 609-614.

[41] Kutzner, I., Stephan, D., Dymke, J., Bender, A., Graichen, F., and Bergmann, G., 2013, "The influence of footwear on knee joint loading during walking--in vivo load measurements with instrumented knee implants," J Biomech, 46(4), pp. 796-800.

[42] Pataky, T. C., 2010, "Generalized n-dimensional biomechanical field analysis using statistical parametric mapping," J Biomech, 43(10), pp. 1976-1982.

[43] Scanlan, S. F., Lai, J., Donahue, J. P., and Andriacchi, T. P., 2012, "Variations in the three-dimensional location and orientation of the ACL in healthy subjects relative to patients after transtibial ACL reconstruction," J Orthop Res, 30(6), pp. 910-918.

[44] Beynnon, B., Yu, J., Huston, D., Fleming, B., Johnson, R., Haugh, L., and Pope, M. H., 1996, "A sagittal plane model of the knee and cruciate ligaments with application of a sensitivity analysis," J Biomech Eng, 118(2), pp. 227-239.

[45] Eby, S. F., Song, P., Chen, S., Chen, Q., Greenleaf, J. F., and An, K. N., 2013, "Validation of shear wave elastography in skeletal muscle," J Biomech, 46(14), pp. 2381-2387.

[46] Hatta, T., Giambini, H., Itoigawa, Y., Hooke, A. W., Sperling, J. W., Steinmann, S. P., Itoi, E., and An, K. N., 2017, "Quantifying extensibility of rotator cuff muscle with tendon rupture using shear wave elastography: A cadaveric study," J Biomech, 61, pp. 131-136.

[47] Low, G., Kruse, S. A., and Lomas, D. J., 2016, "General review of magnetic resonance elastography," World J Radiol, 8(1), pp. 59-72.

[48] Mariappan, Y. K., Glaser, K. J., and Ehman, R. L., 2010, "Magnetic resonance elastography: a review," Clin Anat, 23(5), pp. 497-511.

[49] Slane, L. C., Slane, J. A., D'Hooge, J., and Scheys, L., 2017, "The challenges of measuring in vivo knee collateral ligament strains using ultrasound," J Biomech, 61, pp. 258-262.

[50] Nasseri, A., Khataee, H., Bryant, A. L., Lloyd, D. G., and Saxby, D. J., 2020, "Modelling the loading mechanics of anterior cruciate ligament," Comput Methods Programs Biomed, 184, p. 105098.

[51] van den Bogert, A. J., Reinschmidt, C., and Lundberg, A., 2008, "Helical axes of skeletal knee joint motion during running," J Biomech, 41(8), pp. 1632-1638.

[52] Duthon, V. B., Barea, C., Abrassart, S., Fasel, J. H., Fritschy, D., and Menetrey, J., 2006, "Anatomy of the anterior cruciate ligament," Knee Surg Sports Traumatol Arthrosc, 14(3), pp. 204-213.

Journal of Biomechanical Engineering. Received April 29, 2020;
Accepted manuscript posted October 8, 2020. doi:10.1115/1.4048710

Table 1. The musculotendon units included in each subject-specific musculoskeletal model, as well as associated wrapping surfaces and properties.

Muscle	Abbreviation	Wrap surface properties				
		Wrap surface	Body	Cylinder/sphere	Radius (mm)	Length (mm)
Adductor magnus (lateral)	AM1					
Adductor magnus (medial)	AM2					
Adductor longus	AL					
Adductor brevis	AB					
Gracilis	GRA					
Semimembranosus	SM	Hip extensors at tibia	Leg	Sphere	35	n/a
Semitendinosus	ST					
Biceps femoris- long head	BFL					
Biceps femoris- short head	BFS					
Popliteus	POP					
Sartorius	SAR	Hip extensors at tibia	Leg	Sphere	35	n/a
Rectus femoris	RF					
Vastus lateralis	VL	Knee extensors at femur	Thigh	Cylinder	25	75
Vastus medialis	VM					
Vastus intermedius	VI					
Tibialis anterior	TA					
Extensor digitorum longus	EDL					
Extensor hallucis longus	EHL					
Medial gastrocnemius	MG	Gastrocs at femur/Gastrocs at tibia	Thigh/leg	Cylinder	25	75
Lateral gastrocnemius	LG					
Soleus	SOL					

Journal of Biomechanical Engineering. Received April 29, 2020;
Accepted manuscript posted October 8, 2020. doi:10.1115/1.4048710

576 Table 2. Resting lengths of the aACL in each subject-specific and scaled generic model.

Subject	aACL resting lengths (m)			
	Subject-specific			Scaled-generic
	Initial	+10%	-10%	Initial
S01	0.0352	0.0387	0.0317	0.0283
S02	0.0329	0.0362	0.0296	0.0296
S03	0.0315	0.0347	0.0283	0.0299
S04	0.0306	0.0336	0.0275	0.0295
S05	0.0321	0.0353	0.0289	0.0328
S06	0.0310	0.0341	0.0279	0.0310
S07	0.0307	0.0338	0.0276	0.0320
S08	0.0277	0.0305	0.0249	0.0312
S09	0.0427	0.0469	0.0384	0.0336
S10	0.0382	0.0420	0.0344	0.0330

577

Journal of Biomechanical Engineering. Received April 29, 2020;
Accepted manuscript posted October 8, 2020. doi:10.1115/1.4048710

Table 3. Resting lengths of the pACL in each subject-specific and scaled generic model.

Subject	pACL resting lengths (m)			
	Subject-specific			Scaled-generic
	Initial	+10%	-10%	Initial
S01	0.0270	0.0298	0.0243	0.0215
S02	0.0251	0.0276	0.0226	0.0240
S03	0.0239	0.0263	0.0215	0.0234
S04	0.0216	0.0238	0.0195	0.0195
S05	0.0252	0.0278	0.0227	0.0252
S06	0.0290	0.0319	0.0262	0.0291
S07	0.0258	0.0284	0.0232	0.0245
S08	0.0204	0.0225	0.0184	0.0219
S09	0.0340	0.0373	0.0306	0.0246
S10	0.0276	0.0304	0.0248	0.0239

Journal of Biomechanical Engineering. Received April 29, 2020;
Accepted manuscript posted October 8, 2020. doi:10.1115/1.4048710

Table 4. Subject demographics and root mean squared (RMS) differences of anterior cruciate ligament forces predicted by scaled generic (SG) models relative to subject-specific (SS) models. RMS differences expressed as % of maximum SS force are displayed in parentheses, which highlights the variability of the accuracy of ACL force prediction by the SG models.

Subject	**Sex**	**Age**	**Body mass (kg)**	**Height (cm)**	**RMS difference (SS vs SG; xBW)**	
					aACL	**pACL**
S01	Male	23	90.7	182	0.08 (21%)	0.13 (35%)
S02	Male	26	82.1	173	0.11 (26%)	0.17 (40%)
S03	Male	29	81.1	182	0.10 (25%)	0.18 (43%)
S04	Female	26	71.2	162	0.12 (29%)	0.11 (28%)
S05	Female	23	59.8	170	0.26 (44%)	0.09 (12%)
S06	Female	35	80.2	169	0.13 (31%)	0.09 (33%)
S07	Female	25	80.7	168	0.09 (21%)	0.13 (28%)
S08	Female	26	40.6	162	0.27 (31%)	0.09 (10%)
S09	Male	26	84.8	187	0.21 (64%)	0.06 (15%)
S10	Male	34	82.5	192	0.12 (30%)	0.05 (17%)

Journal of Biomechanical Engineering. Received April 29, 2020;
Accepted manuscript posted October 8, 2020. doi:10.1115/1.4048710

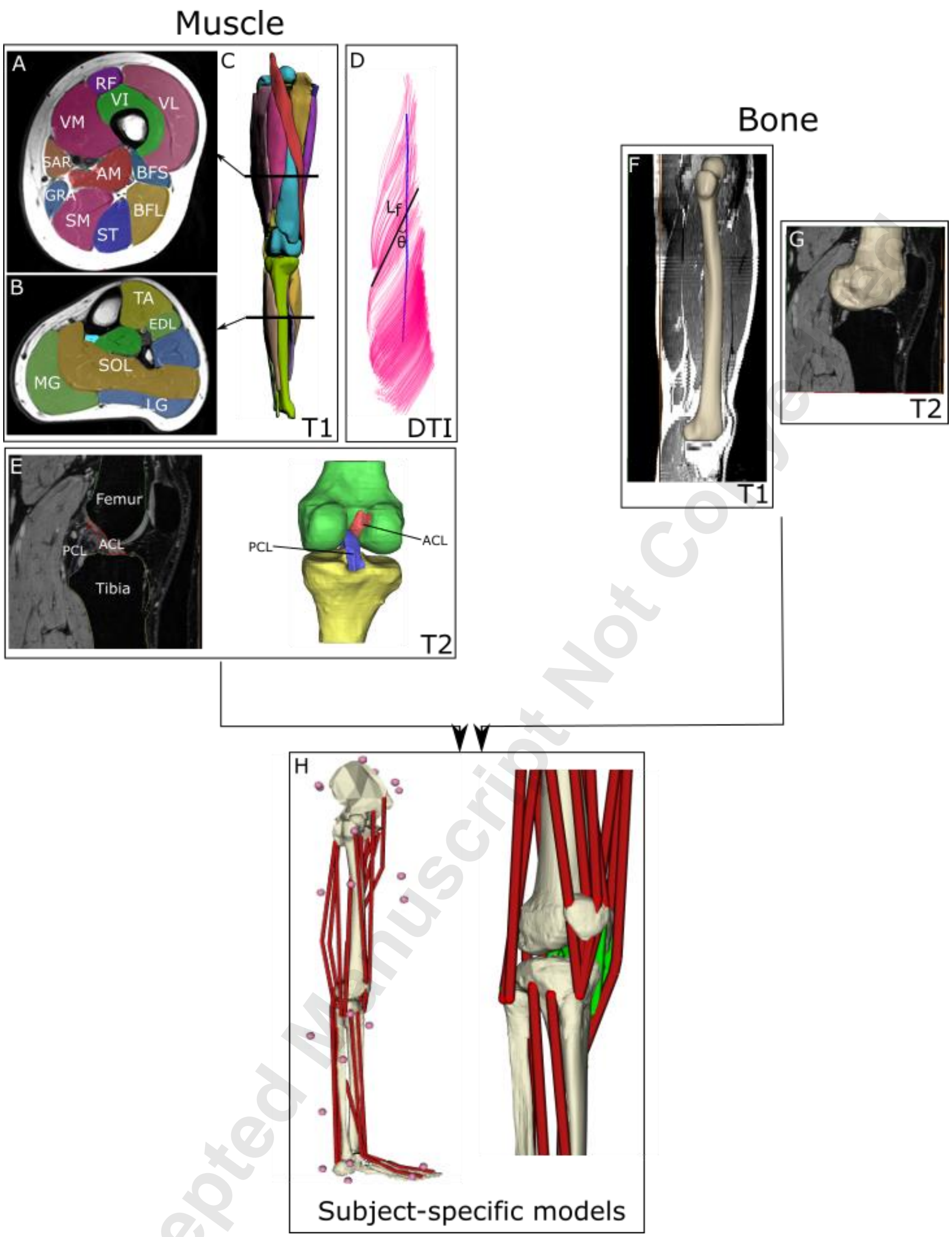

Figure 1. Framework for constructing subject-specific lower limb musculoskeletal models from T1, T2 magnetic resonance imaging (MRI) and diffusion tensor imaging (DTI). Muscles, ligaments and bones were manually segmented from these images to create 3D meshes, and musclulotendon unit and ligament attachments and via points were manually placed based on these meshes. Muscle force generating properties for each individual were determined for 20 lower limb muscles using a validated framework of DTI and fiber tractography [27], which have formed a reference data set of *in vivo* muscle architetcure data [28].

Journal of Biomechanical Engineering. Received April 29, 2020;
Accepted manuscript posted October 8, 2020. doi:10.1115/1.4048710

58

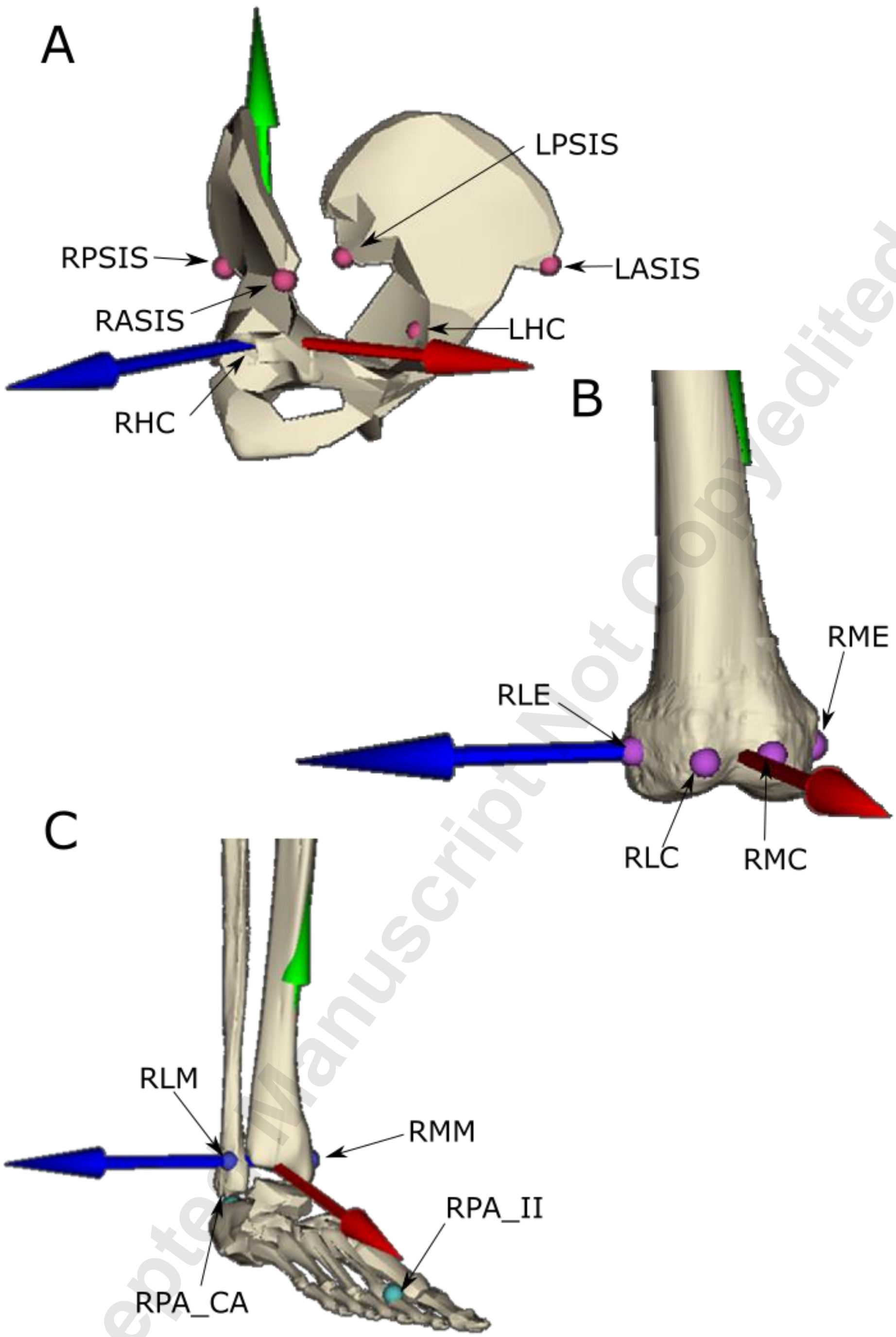

Figure 2. Joint centers for the hip (A), knee (B) and ankle (C) joints in each subject-specific musculoskeletal model constructed in NMSBuilder [29]. The position and orientation were determined by the position of anatomical landmarks defined by the International Society of Biomechanics [38]. The coordinate system origin for each body in the model (pelvis, thigh, leg and foot) was set as the joint center of the respective parent joint. RPSIS/LPSIS- right/left posterior superior iliac spine, RASIS/LASIS- right/left anterior superior iliac spine, RHC/LHC- right/left hip center, RLE/RME- right lateral/medial femoral epicondyle, RLC/RMC- right lateral/medial femoral condyle, RLM/RMM- right lateral/medial malleolus, RPA_CA- right posterior aspect of calcaneus, RPA_II- right posterior aspect of second metatarsal.

Journal of Biomechanical Engineering. Received April 29, 2020;
Accepted manuscript posted October 8, 2020. doi:10.1115/1.4048710

589

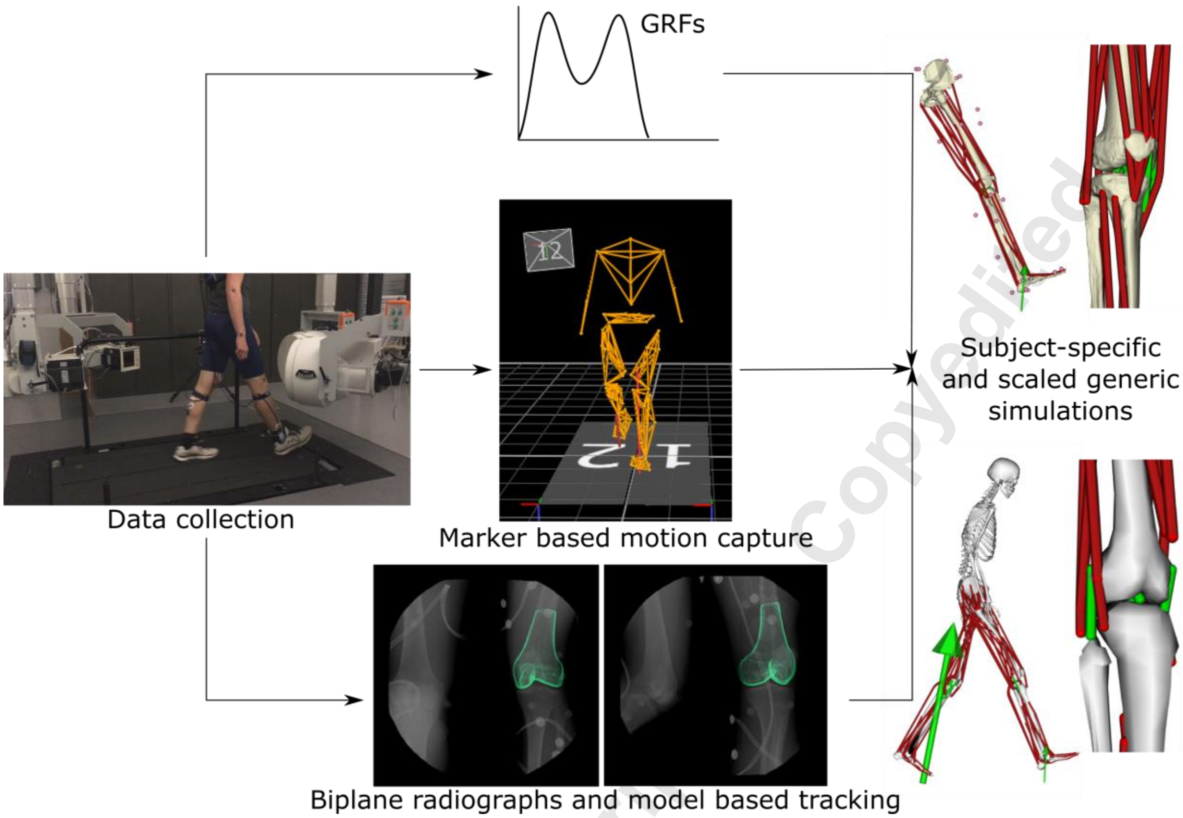

Figure 3. Workflow to create subject-specific and scaled generic musculoskeletal simulations from kinematic and kinetic data collection. Whole body kinematics were obtained from maker based motion capture, while precise 6 degree of freedom knee joint kinemaitcs were obtained from dynamic biplane radiography and a validated model based tracking algorithm [24]. Combined with ground reaction forces (GRFs), these data were used to develop simulations of treadmill walking with subject-specfic and scaled genericmusculoskeletal models.

Journal of Biomechanical Engineering. Received April 29, 2020;
Accepted manuscript posted October 8, 2020. doi:10.1115/1.4048710

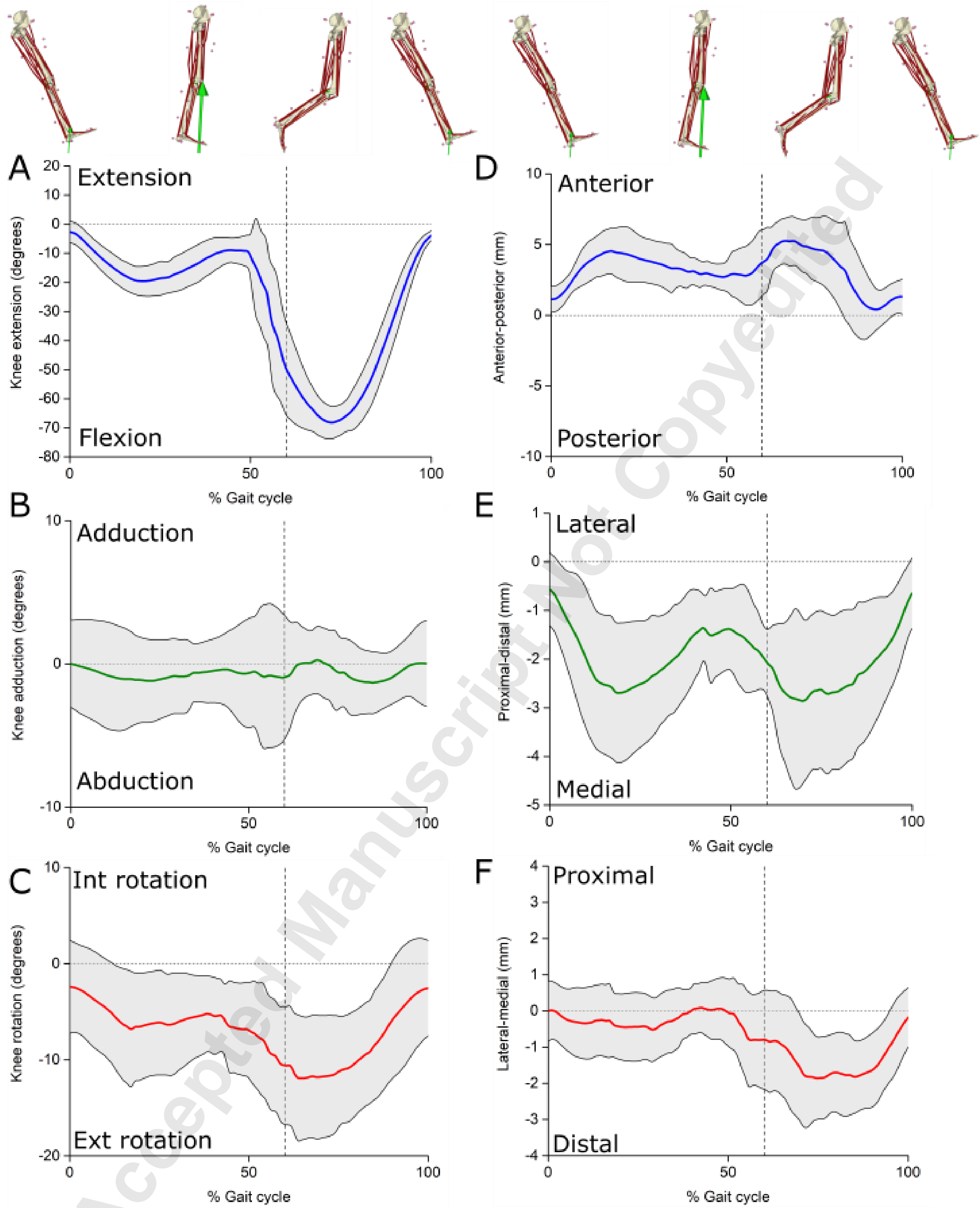

Figure 4. Mean (± 1 SD) knee extension (A), adduction (B) and internal rotation (C) joint angles and anterior-posterior (D), lateral-medial (E) and proximal-distal (F) tibial translations determined from dynamic biplane radiography (DBR), biplane radiographs and model based tracking, and input into subject-specific and scaled-generic musculoskeletal models. The vertical dashed line indicates average toe-off time.

Journal of Biomechanical Engineering. Received April 29, 2020;
Accepted manuscript posted October 8, 2020. doi:10.1115/1.4048710

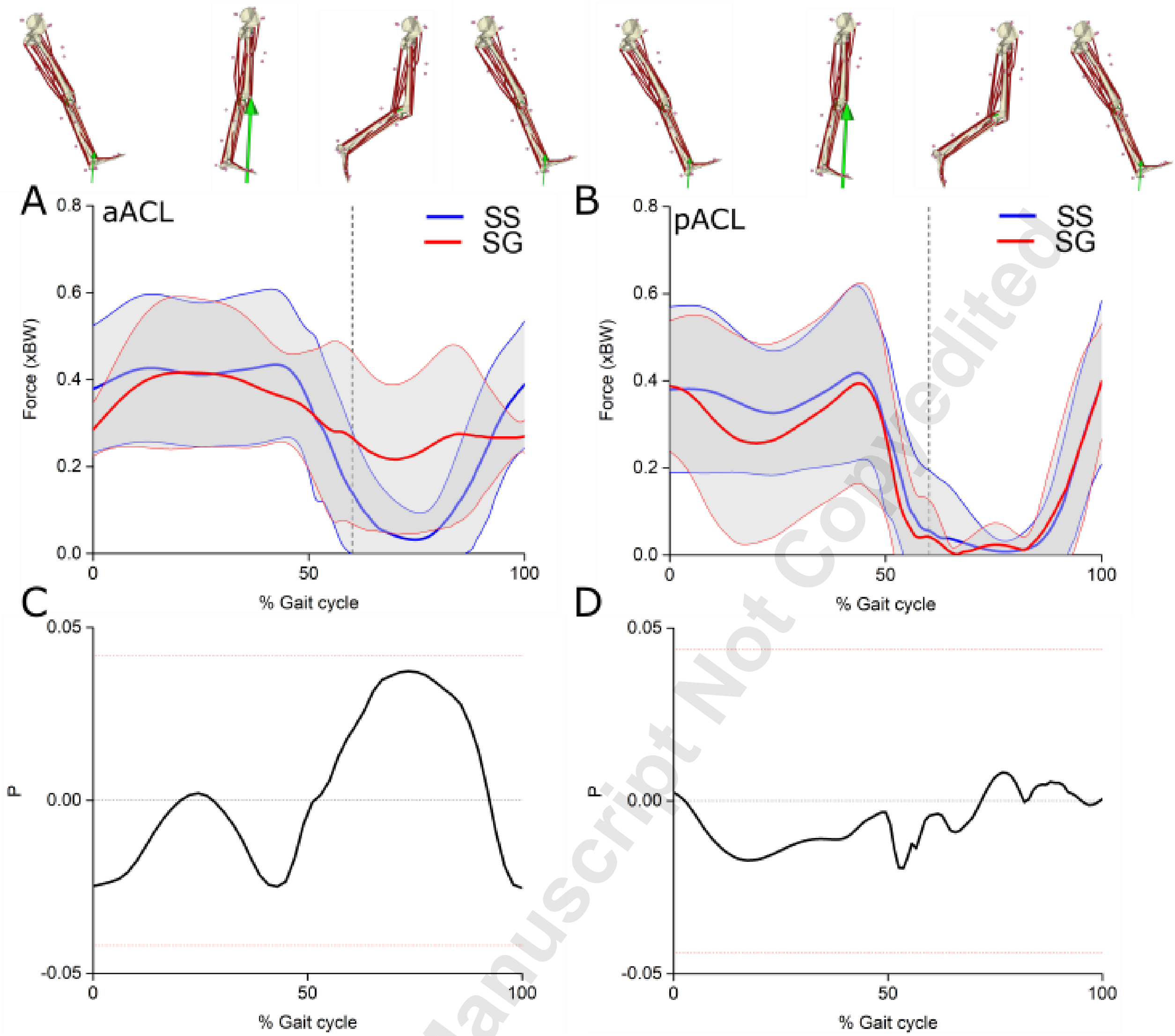

Figure 5. Comparison of mean (±1 SD) forces (xBW) in the anterior-medial bundle of the anterior cruciate ligament (aACL; A) and posterior-lateral bundle (pACL; B) as predicted from subject-specific (SS) and scaled generic (SG) simulations of one stride of walking gait. The vertical dashed line indicates average toe-off time. SPM{t} values (aACL, C; pACL, D) through the gait cycle indicate the level of statistical significance between the model predictions. Red horizontal dashed lines represent respective thresholds of statistical significance (SPM{t} > 4.18 or < -4.18 for the aACL, and > 4.37 or < -4.37 for the pACL).

Journal of Biomechanical Engineering. Received April 29, 2020;
Accepted manuscript posted October 8, 2020. doi:10.1115/1.4048710

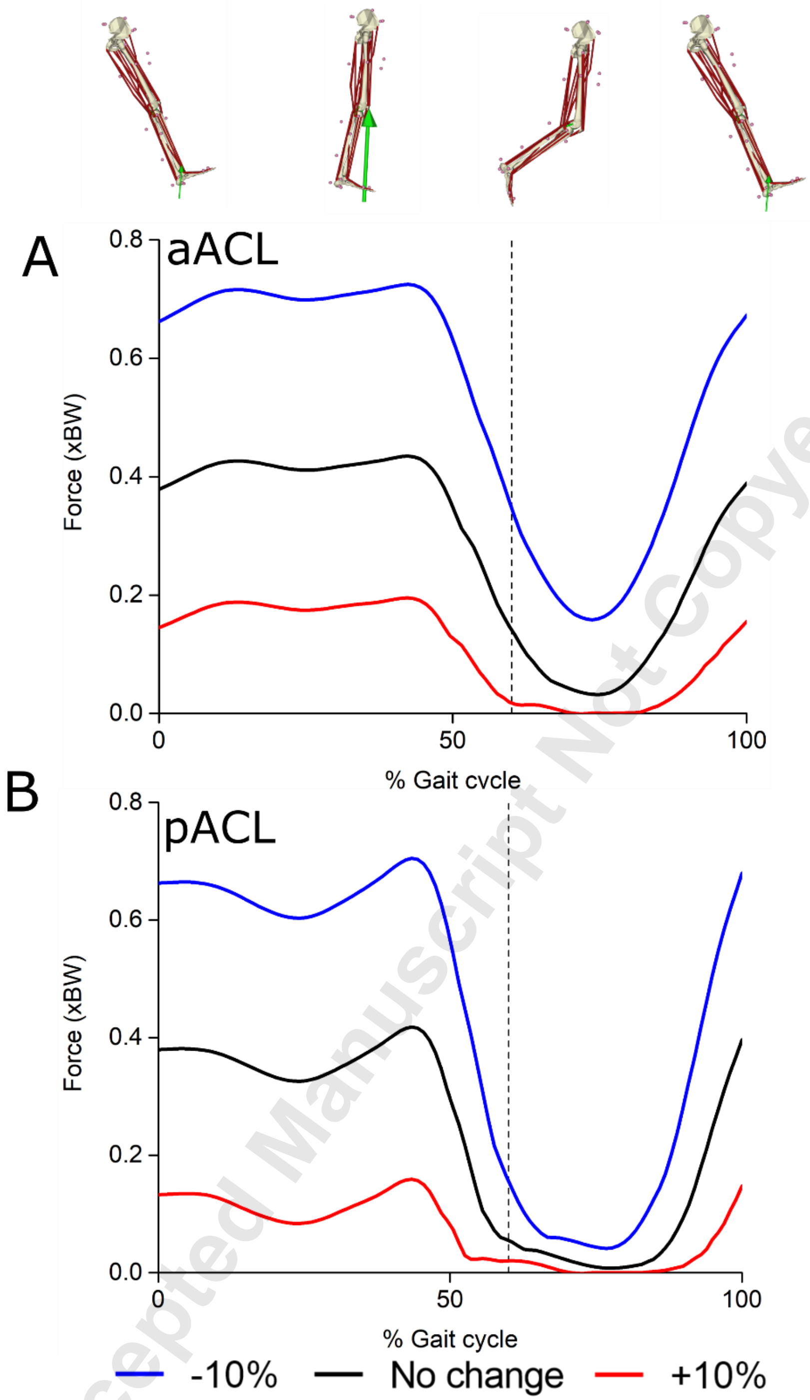

Figure 6. Sensitivity analysis of mean forces (xBW) in the anterior-medial bundle of the anterior cruciate ligament (aACL; A) and posterior-lateral bundle (pACL; B) predicted from subject-specific (SS) simulations of the stride of walking gait, where resting lengths were changed ±10% from the original value. The vertical dashed line indicates average toe-off time.

Journal of Biomechanical Engineering. Received April 29, 2020;
Accepted manuscript posted October 8, 2020. doi:10.1115/1.4048710

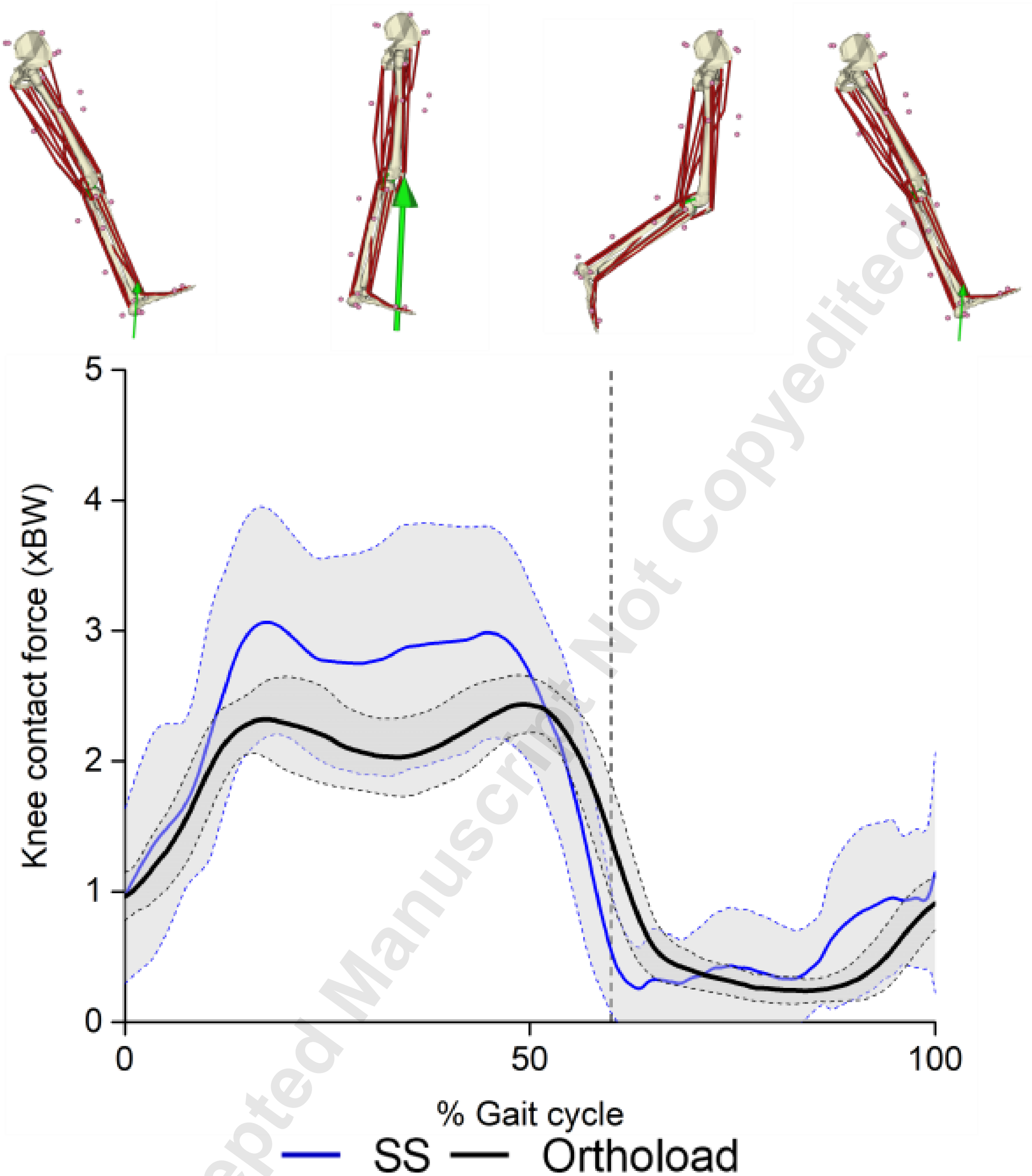

Figure 7. Mean (± standard deviation) knee joint contact forces predicted by the subject-specific (SS) models using the Joint Reaction Analysis in Opensim, compared to *in vivo* knee contact forces measured using instrumented knee joint replacements [41]. The vertical dashed line indicates the average toe-off time in the SS simulations.

Journal of Biomechanical Engineering. Received April 29, 2020;
Accepted manuscript posted October 8, 2020. doi:10.1115/1.4048710

Table S1. *Muscle force generating properties included in the model of Subject 01 (Male, Age- 23y/o, Body mass- 90.7kg, Height- 182cm, Lower limb mass- 6.9kg, Lower limb length- 87.2cm). L_f- Optimal fiber length. L_{ts}- Tendon slack length.*

Muscle	Abbreviation	L_f (mm)	Pennation angle (°)	Max force (N)	L_{ts} (m)
Adductor magnus (lateral)	**AM1**	228	18	630	0.16
Adductor magnus (medial)	**AM2**	228	18	630	0.16
Adductor longus	**AL**	102	13	652	0.10
Adductor brevis	**AB**	61	12	587	0.26
Gracilis	**GRA**	226	7	185	0.15
Semimembranosus	**SM**	105	20	733	0.35
Semitendinosus	**ST**	169	14	470	0.29
Biceps femoris- long head	**BFL**	128	18	720	0.32
Biceps femoris- short head	**BFS**	107	12	368	0.14
Popliteus	**POP**	74	19	99	0.08
Sartorius	**SAR**	453	0	126	0.02
Rectus femoris	**RF**	111	10	856	0.41
Vastus lateralis	**VL**	115	15	2280	0.42
Vastus medialis	**VM**	119	18	1536	0.38
Vastus intermedius	**VI**	182	11	1177	0.35
Tibialis anterior	**TA**	175	6	248	0.24
Extensor digitorum longus	**EDL**	181	7	125	0.30
Extensor hallucis longus	**EHL**	123	5	71	0.20
Medial gastrocnemius	**MG**	79	11	1052	0.40
Lateral gastrocnemius	**LG**	143	7	293	0.35
Soleus	**SOL**	196	13	846	0.18

Journal of Biomechanical Engineering. Received April 29, 2020;
Accepted manuscript posted October 8, 2020. doi:10.1115/1.4048710

Table S2. *Muscle force generating properties included in the model of Subject 02 (Male, Age- 26y/o, Body mass- 82.1kg, Height- 173cm, Lower limb mass- 5.4kg, Lower limb length- 82.5cm). L_f- Optimal fiber length. L_{ts}- Tendon slack length*

Muscle	Abbreviation	L_f (mm)	Pennation angle (°)	Max force (N)	L_{ts} (m)
Adductor magnus (lateral)	**AM1**	311	15	305	0.16
Adductor magnus (medial)	**AM2**	311	15	305	0.16
Adductor longus	**AL**	125	11	383	0.10
Adductor brevis	**AB**	104	15	281	0.26
Gracilis	**GRA**	157	7	154	0.15
Semimembranosus	**SM**	170	10	410	0.23
Semitendinosus	**ST**	99	10	578	0.21
Biceps femoris- long head	**BFL**	190	22	286	0.22
Biceps femoris- short head	**BFS**	75	9	304	0.14
Popliteus	**POP**	58	11	81	0.05
Sartorius	**SAR**	400	0	100	0.02
Rectus femoris	**RF**	126	10	580	0.41
Vastus lateralis	**VL**	211	27	817	0.35
Vastus medialis	**VM**	103	21	1360	0.39
Vastus intermedius	**VI**	128	21	1387	0.35
Tibialis anterior	**TA**	134	12	327	0.24
Extensor digitorum longus	**EDL**	103	12	264	0.30
Extensor hallucis longus	**EHL**	81	10	119	0.20
Medial gastrocnemius	**MG**	88	20	755	0.33
Lateral gastrocnemius	**LG**	74	16	647	0.31
Soleus	**SOL**	182	10	927	0.18

Journal of Biomechanical Engineering. Received April 29, 2020;
Accepted manuscript posted October 8, 2020. doi:10.1115/1.4048710

Table S3. *Muscle force generating properties included in the model of Subject 03 (Male, Age- 29y/o, Body mass- 81.1kg, Height- 182cm, Lower limb mass- 5.3kg, Lower limb length- 84.8cm). L_f- Optimal fiber length. L_{ts}- Tendon slack length.*

Muscle	Abbreviation	L_f (mm)	Pennation angle (°)	Max force (N)	L_{ts} (m)
Adductor magnus (lateral)	**AM1**	271	12	289	0.16
Adductor magnus (medial)	**AM2**	271	12	289	0.16
Adductor longus	**AL**	105	14	572	0.17
Adductor brevis	**AB**	73	9	350	0.09
Gracilis	**GRA**	212	0	141	0.15
Semimembranosus	**SM**	187	13	403	0.22
Semitendinosus	**ST**	158	7	487	0.27
Biceps femoris- long head	**BFL**	213	8	336	0.20
Biceps femoris- short head	**BFS**	108	10	299	0.10
Popliteus	**POP**	95	6	59	0.03
Sartorius	**SAR**	434	0	104	0.02
Rectus femoris	**RF**	121	8	781	0.43
Vastus lateralis	**VL**	213	13	918	0.33
Vastus medialis	**VM**	177	13	680	0.35
Vastus intermedius	**VI**	144	10	1225	0.35
Tibialis anterior	**TA**	167	7	274	0.20
Extensor digitorum longus	**EDL**	127	8	168	0.30
Extensor hallucis longus	**EHL**	132	8	57	0.20
Medial gastrocnemius	**MG**	105	8	656	0.29
Lateral gastrocnemius	**LG**	145	9	258	0.27
Soleus	**SOL**	108	12	1284	0.22

Journal of Biomechanical Engineering. Received April 29, 2020;
Accepted manuscript posted October 8, 2020. doi:10.1115/1.4048710

Table S4. *Muscle force generating properties included in the model of Subject 04 (Female, Age- 26y/o, Body mass-71.2kg, Height- 162cm, Lower limb mass- 4.4kg, Lower limb length- 80.7cm). L_f- Optimal fiber length. L_{ts}- Tendon slack length.*

Muscle	Abbreviation	L_f (mm)	Pennation angle (°)	Max force (N)	L_{ts} (m)
Adductor magnus (lateral)	**AM1**	146	12	552	0.16
Adductor magnus (medial)	**AM2**	146	12	552	0.16
Adductor longus	**AL**	51	11	567	0.17
Adductor brevis	**AB**	34	14	554	0.08
Gracilis	**GRA**	175	6	129	0.15
Semimembranosus	**SM**	127	9	611	0.25
Semitendinosus	**ST**	228	5	202	0.24
Biceps femoris- long head	**BFL**	241	10	197	0.20
Biceps femoris- short head	**BFS**	137	9	197	0.11
Popliteus	**POP**	55	11	63	0.08
Sartorius	**SAR**	389	0	130	0.02
Rectus femoris	**RF**	150	7	426	0.43
Vastus lateralis	**VL**	230	15	804	0.33
Vastus medialis	**VM**	210	11	565	0.35
Vastus intermedius	**VI**	215	11	644	0.35
Tibialis anterior	**TA**	109	9	259	0.20
Extensor digitorum longus	**EDL**	130	7	127	0.30
Extensor hallucis longus	**EHL**	128	5	47	0.20
Medial gastrocnemius	**MG**	82	11	688	0.29
Lateral gastrocnemius	**LG**	74	7	513	0.27
Soleus	**SOL**	118	11	894	0.21

Journal of Biomechanical Engineering. Received April 29, 2020;
Accepted manuscript posted October 8, 2020. doi:10.1115/1.4048710

Table S5. *Muscle force generating properties included in the model of Subject 05 (Female, Age- 23y/o, Body mass-59.8kg, Height- 170cm, Lower limb mass- 4.2kg, Lower limb length- 83.0cm). L_f- Optimal fiber length. L_{ts}- Tendon slack length.*

Muscle	Abbreviation	L_f (mm)	Pennation angle (°)	Max force (N)	L_{ts} (m)
Adductor magnus (lateral)	**AM1**	177	14	314	0.25
Adductor magnus (medial)	**AM2**	177	14	314	0.25
Adductor longus	**AL**	145	13	296	0.17
Adductor brevis	**AB**	100	10	295	0.09
Gracilis	**GRA**	109	6	224	0.35
Semimembranosus	**SM**	176	10	359	0.25
Semitendinosus	**ST**	237	7	224	0.25
Biceps femoris- long head	**BFL**	228	9	200	0.20
Biceps femoris- short head	**BFS**	107	8	213	0.13
Popliteus	**POP**	94	9	34	0.03
Sartorius	**SAR**	394	0	86	0.02
Rectus femoris	**RF**	140	8	580	0.35
Vastus lateralis	**VL**	152	16	1054	0.33
Vastus medialis	**VM**	146	13	665	0.28
Vastus intermedius	**VI**	165	14	838	0.35
Tibialis anterior	**TA**	100	7	386	0.20
Extensor digitorum longus	**EDL**	101	5	260	0.40
Extensor hallucis longus	**EHL**	68	4	23	0.28
Medial gastrocnemius	**MG**	89	9	673	0.29
Lateral gastrocnemius	**LG**	128	7	234	0.27
Soleus	**SOL**	140	12	788	0.24

Journal of Biomechanical Engineering. Received April 29, 2020;
Accepted manuscript posted October 8, 2020. doi:10.1115/1.4048710

Table S6. *Muscle force generating properties included in the model of Subject 06 (Female, Age- 35y/o, Body mass- 80.2kg, Height- 169cm, Lower limb mass- 4.6kg, Lower limb length- 78.7cm). L_f- Optimal fiber length. L_{ts}- Tendon slack length.*

Muscle	Abbreviation	L_f (mm)	Pennation angle (°)	Max force (N)	L_{ts} (m)
Adductor magnus (lateral)	**AM1**	250	11	342	0.17
Adductor magnus (medial)	**AM2**	250	11	342	0.17
Adductor longus	**AL**	136	10	265	0.17
Adductor brevis	**AB**	77	11	477	0.18
Gracilis	**GRA**	156	8	165	0.22
Semimembranosus	**SM**	193	10	412	0.26
Semitendinosus	**ST**	213	8	197	0.21
Biceps femoris- long head	**BFL**	210	8	266	0.20
Biceps femoris- short head	**BFS**	118	7	172	0.20
Popliteus	**POP**	60	9	76	0.10
Sartorius	**SAR**	378	0	108	0.02
Rectus femoris	**RF**	218	8	277	0.30
Vastus lateralis	**VL**	274	16	559	0.30
Vastus medialis	**VM**	147	15	739	0.31
Vastus intermedius	**VI**	228	10	678	0.30
Tibialis anterior	**TA**	101	8	375	0.20
Extensor digitorum longus	**EDL**	136	8	153	0.30
Extensor hallucis longus	**EHL**	97	8	55	0.20
Medial gastrocnemius	**MG**	121	7	613	0.28
Lateral gastrocnemius	**LG**	159	7	226	0.23
Soleus	**SOL**	157	11	815	0.20

Journal of Biomechanical Engineering. Received April 29, 2020;
Accepted manuscript posted October 8, 2020. doi:10.1115/1.4048710

Table S7. *Muscle force generating properties included in the model of Subject 07 (Female, Age- 25y/o, Body mass- 80.7kg, Height- 168cm, Lower limb mass- 3.3kg, Lower limb length- 77.9cm). L_f- Optimal fiber length. L_{ts}- Tendon slack length.*

Muscle	Abbreviation	L_f (mm)	Pennation angle (°)	Max force (N)	L_{ts} (m)
Adductor magnus (lateral)	**AM1**	307	9	161	0.25
Adductor magnus (medial)	**AM2**	307	9	161	0.25
Adductor longus	**AL**	126	9	209	0.17
Adductor brevis	**AB**	71	12	272	0.09
Gracilis	**GRA**	130	8	137	0.30
Semimembranosus	**SM**	108	12	437	0.28
Semitendinosus	**ST**	155	7	232	0.28
Biceps femoris- long head	**BFL**	145	11	290	0.22
Biceps femoris- short head	**BFS**	150	9	179	0.13
Popliteus	**POP**	87	12	34	0.03
Sartorius	**SAR**	350	0	111	0.02
Rectus femoris	**RF**	131	5	347	0.35
Vastus lateralis	**VL**	171	10	713	0.30
Vastus medialis	**VM**	189	9	392	0.25
Vastus intermedius	**VI**	195	7	454	0.28
Tibialis anterior	**TA**	134	5	260	0.20
Extensor digitorum longus	**EDL**	153	7	97	0.40
Extensor hallucis longus	**EHL**	116	6	54	0.28
Medial gastrocnemius	**MG**	83	8	777	0.29
Lateral gastrocnemius	**LG**	53	9	516	0.27
Soleus	**SOL**	170	8	595	0.24

Journal of Biomechanical Engineering. Received April 29, 2020;
Accepted manuscript posted October 8, 2020. doi:10.1115/1.4048710

Table S8. *Muscle force generating properties included in the model of Subject 08 (Female, Age- 26y/o, Body mass- 40.6kg, Height- 162cm, Lower limb mass- 3.1kg, Lower limb length- 73.1cm). L_f- Optimal fiber length. L_{ts}- Tendon slack length.*

Muscle	Abbreviation	L_f (mm)	Pennation angle (°)	Max force (N)	L_{ts} (m)
Adductor magnus (lateral)	**AM1**	120	10	451	0.17
Adductor magnus (medial)	**AM2**	120	10	451	0.17
Adductor longus	**AL**	77	10	384	0.17
Adductor brevis	**AB**	53	9	369	0.10
Gracilis	**GRA**	74	8	173	0.28
Semimembranosus	**SM**	114	15	393	0.27
Semitendinosus	**ST**	134	8	244	0.25
Biceps femoris- long head	**BFL**	237	10	146	0.19
Biceps femoris- short head	**BFS**	82	9	248	0.11
Popliteus	**POP**	79	8	28	0.05
Sartorius	**SAR**	407	0	51	0.02
Rectus femoris	**RF**	63	8	721	0.40
Vastus lateralis	**VL**	187	13	614	0.30
Vastus medialis	**VM**	114	12	714	0.30
Vastus intermedius	**VI**	115	11	883	0.30
Tibialis anterior	**TA**	140	6	182	0.20
Extensor digitorum longus	**EDL**	143	7	128	0.30
Extensor hallucis longus	**EHL**	79	7	57	0.20
Medial gastrocnemius	**MG**	69	11	551	0.25
Lateral gastrocnemius	**LG**	88	12	230	0.27
Soleus	**SOL**	149	16	630	0.21

Journal of Biomechanical Engineering. Received April 29, 2020;
Accepted manuscript posted October 8, 2020. doi:10.1115/1.4048710

671 Table S9. *Muscle force generating properties included in the model of Subject 09 (Male, Age- 26y/o, Body*
672 *mass- 84.8kg, Height- 187cm, Lower limb mass- 6.4kg, Lower limb length- 90.8cm). L_f- Optimal fiber*
673 *length. L_{ts}- Tendon slack length.*

Muscle	Abbreviation	L_f (mm)	Pennation angle (°)	Max force (N)	L_{ts} (m)
Adductor magnus (lateral)	**AM1**	262	9	390	0.17
Adductor magnus (medial)	**AM2**	262	9	390	0.17
Adductor longus	**AL**	112	14	684	0.17
Adductor brevis	**AB**	99	9	310	0.10
Gracilis	**GRA**	263	7	176	0.23
Semimembranosus	**SM**	247	11	432	0.25
Semitendinosus	**ST**	233	7	323	0.20
Biceps femoris- long head	**BFL**	245	9	244	0.19
Biceps femoris- short head	**BFS**	109	10	343	0.11
Popliteus	**POP**	75	9	82	0.07
Sartorius	**SAR**	434	0	147	0.02
Rectus femoris	**RF**	209	9	497	0.35
Vastus lateralis	**VL**	214	14	1083	0.30
Vastus medialis	**VM**	224	14	724	0.30
Vastus intermedius	**VI**	227	9	762	0.30
Tibialis anterior	**TA**	149	5	304	0.20
Extensor digitorum longus	**EDL**	183	5	167	0.30
Extensor hallucis longus	**EHL**	143	5	41	0.20
Medial gastrocnemius	**MG**	145	7	637	0.28
Lateral gastrocnemius	**LG**	188	9	311	0.27
Soleus	**SOL**	155	14	1244	0.24

674

Journal of Biomechanical Engineering. Received April 29, 2020;
Accepted manuscript posted October 8, 2020. doi:10.1115/1.4048710

Table S10. *Muscle force generating properties included in the model of Subject 10 (Male, Age- 34y/o, Body mass- 82.5kg, Height- 192cm, Lower limb mass- 4.9kg, Lower limb length- 90.2cm). L_f- Optimal fiber length. L_{ts}- Tendon slack length*

Muscle	Abbreviation	L_f (mm)	Pennation angle (°)	Max force (N)	L_{ts} (m)
Adductor magnus (lateral)	**AM1**	239	12	350	0.17
Adductor magnus (medial)	**AM2**	239	12	350	0.17
Adductor longus	**AL**	124	14	397	0.17
Adductor brevis	**AB**	90	14	307	0.10
Gracilis	**GRA**	223	8	109	0.23
Semimembranosus	**SM**	152	10	493	0.29
Semitendinosus	**ST**	209	6	261	0.24
Biceps femoris- long head	**BFL**	207	9	309	0.23
Biceps femoris- short head	**BFS**	99	11	225	0.15
Popliteus	**POP**	65	8	48	0.07
Sartorius	**SAR**	436	0	86	0.02
Rectus femoris	**RF**	153	8	495	0.38
Vastus lateralis	**VL**	196	13	776	0.30
Vastus medialis	**VM**	158	15	748	0.35
Vastus intermedius	**VI**	215	11	765	0.30
Tibialis anterior	**TA**	163	5	249	0.20
Extensor digitorum longus	**EDL**	126	7	223	0.30
Extensor hallucis longus	**EHL**	97	7	63	0.20
Medial gastrocnemius	**MG**	103	8	712	0.28
Lateral gastrocnemius	**LG**	166	7	246	0.27
Soleus	**SOL**	89	10	1653	0.24